Lawrence Berkeley National Laboratory

Title
Evolution of Ionomer Morphology from Dispersion to Film: An in Situ X-ray Study

Authors
Dudenas, Peter J
Kusoglu, Ahmet

Evolution of Ionomer Morphology from Dispersion to Film: An in-situ X-Ray Study

Peter J. Dudenas[1,2] and Ahmet Kusoglu[2,*]

[1] Chemical and Biomolecular Engineering, University of California Berkeley, Berkeley, CA, 94720
[2] Energy Conversion Group, Lawrence Berkeley National Laboratory, Berkeley, CA, 94720

*Author to whom correspondence should be addressed: akusoglu@lbl.gov

Abstract

Ion-conducting polymers (ionomers) have been extensively studied in solution, as membranes and substrate-supported thin films for various electrochemical energy conversion devices, including fuel-cells and electrolyzers. Formation of an ionomer film from a solution, however, is not well understood, despite its importance for fabrication of electrodes in energy devices. Here, the evolution of the perfluorinated sulfonic acid (PFSA) morphology upon casting from a solution is observed using *in-situ* grazing-incidence small- and wide-angle x-ray scattering (GISAXS/GIWAXS). Aggregate interactions in dispersion directly impact the hydrophilic-domain network of the cast film and the onset of crystallization occur simultaneously with the solution-to-film transition, but continue to evolve on different timescales. In addition, confinement is shown to induce anisotropic morphology at multiple lengthscales. These results show promise for elucidating the role of casting parameters, drying protocols, and ionomer-solvent interactions in governing film morphology and open new avenues for establishing structure/processing/property relationships for ionomer films and modifying their transport functionality at catalytic interfaces.

Keywords: Thin Films, PFSA Ionomers, Casting, GISAXS, Nanostructure, Functional Interfaces

Main Text

Perfluorinated sulfonic acid polymers (PFSAs) are a class of ion-conducting polymer (ionomer) widely used in energy conversion devices such as fuel cells and electrolyzers. PFSAs chemical structure consists of a hydrophobic polytetrafluoroethylene (PTFE) backbone, providing mechanical stability, with pendant side chains terminated in a sulfonic acid group (see Figure S1 in SI). This amphiphilic nature leads to phase-segregation, and upon hydration, dissociated protons conduct through hydrophilic domains of a bi-continuous network. The unique structure-driven multi-functionality of PFSA ionomers makes it the prototypical material for energy conversion devices; thus, there is a rich literature on PFSAs as a bulk membrane (10-50 μm).[1,2] Moreover, there has been a growing interest in understanding ionomers as thin-films (< 100 nm thickness), which stems from the need to understand their behavior in the catalyst layers (CLs) of a fuel cell or electrolyzer.[1-5] In CLs, ionomer thin-films act as a binder and conducting media, transporting reactants and products to and from the catalytic sites (e.g., platinum) supported on carbon.[3,6] CLs are cast from inks, where ionomer and catalyst-coated carbon particles are dispersed in a mixture of solvents, typically water/alcohol mixtures. To date, these inks and CLs have been empirically formulated, relying only on the end performance for guidance.[3-6] In an effort to understand the underlying science governing CL formation and, in turn, performance, more recent studies focused on ionomer/solvent interactions, ink formulations, and structure.[4,5,7-12] Furthermore, the dynamic processes that occur when inks are cast is an essential step in CL formation. In particular, it is important to know how the more volatile solvents preferentially evaporate first and affect ionomer structure and aggregation behavior in the drying ink. Then, to what extent do the structures in the colloidal state persist in the cast film and impact ionomer properties and performance? To begin to answer these questions, we start with a model system of PFSA ionomer in solution. Understanding gained

2

from this model system can be applied to more complex ink systems and other ionomer-solvent compositions and inform the relative impact of components and their binary interactions on CL formation. Herein, we report the morphological changes during film formation of Nafion PFSA ionomer *in-situ* using grazing incidence x-ray scattering (GIXS).

A number of studies have utilized *in-situ* GIXS to understand the formation of organic electronics. Films are prepared using either a slot-die printer,[13-15] spin coater,[16, 17] or spray-coater[18] and morphological data is collected as solvent evaporates and the film dries. These studies have shown that solvent, temperature, and organic composition affect both the transient and final morphologies, the latter of which can be correlated to device performance.[19] Ionomers present a distinctly different system to study, where protons (or ions) are the conducting species and conduction occurs through the water-filled domains of the phase-separated nano-morphology.[1] A slot-die printer is used to cast 5 wt% Nafion ionomer solution onto a diced silicon wafer, and morphology of the solution/film is collected via GIXS as a function of time (Figure 1a). Films were cast and imaged *in-situ* at small and large sample-to-detector distances to monitor the morphology evolution at multiple lengthscales.
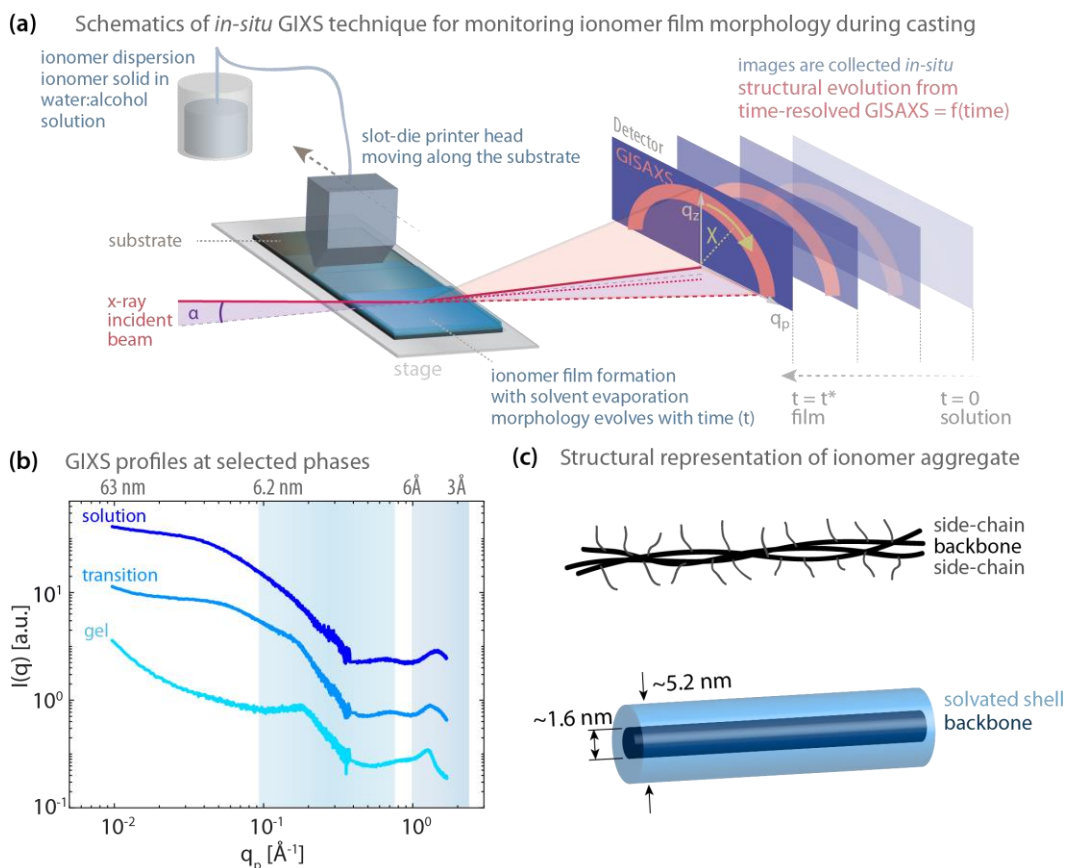
(a) Schematics of *in-situ* GIXS technique for monitoring ionomer film morphology during casting

ionomer dispersion
ionomer solid in water:alcohol solution

slot-die printer head moving along the substrate

Detector GISAXS

q_z

χ

images are collected *in-situ*
structural evolution from time-resolved GISAXS = f(time)

substrate

x-ray incident beam

α

stage

q_p

ionomer film formation with solvent evaporation morphology evolves with time (t)

t = t*
film

t = 0
solution

(b) GIXS profiles at selected phases

63 nm   6.2 nm   6Å   3Å

solution

transition

gel

$I(q)$ [a.u.]

q_p [Å^{-1}]

(c) Structural representation of ionomer aggregate

side-chain
backbone
side-chain

~5.2 nm

~1.6 nm

solvated shell
backbone

Figure 1. (a) Schematic of *in-situ* printing technique for monitoring ionomer film morphology. (b) Composite GIXS linecuts showing evolution of morphology across lengthscales. (c) Schematic of Nafion aggregate and core-shell cylinder model used to fit the solution data.

Immediately after casting, the "film" is still in a solution state and from prior studies, a rod-like aggregate of polymer chains is expected.[20-22] Figure 1b shows merged horizontal line-cuts from both GISAXS and GIWAXS for the early-time morphology. To accurately reproduce the shoulder at ~0.3 Å^{-1} and peak at ~0.6 Å^{-1}, a core-shell cylinder model is chosen (see SI for fit). The extracted parameters indicate a dense core of PTFE backbone with a radius of ~0.8 nm, and a much less dense shell layer with a thickness of ~1.8 nm (Figure 1c). The shell is composed of side chain, solvated ionic moieties and solvent, and represents an average electron density of these components. This cross-sectional representative volume has previously been employed for SAXS, and is now confirmed in this study with the higher-q data obtained from GIWAXS.

While the core-shell cylinder can also be fit to the low-q region, the initial solution is 5 wt% and

therefore a structure factor is expected due to interparticle interactions.
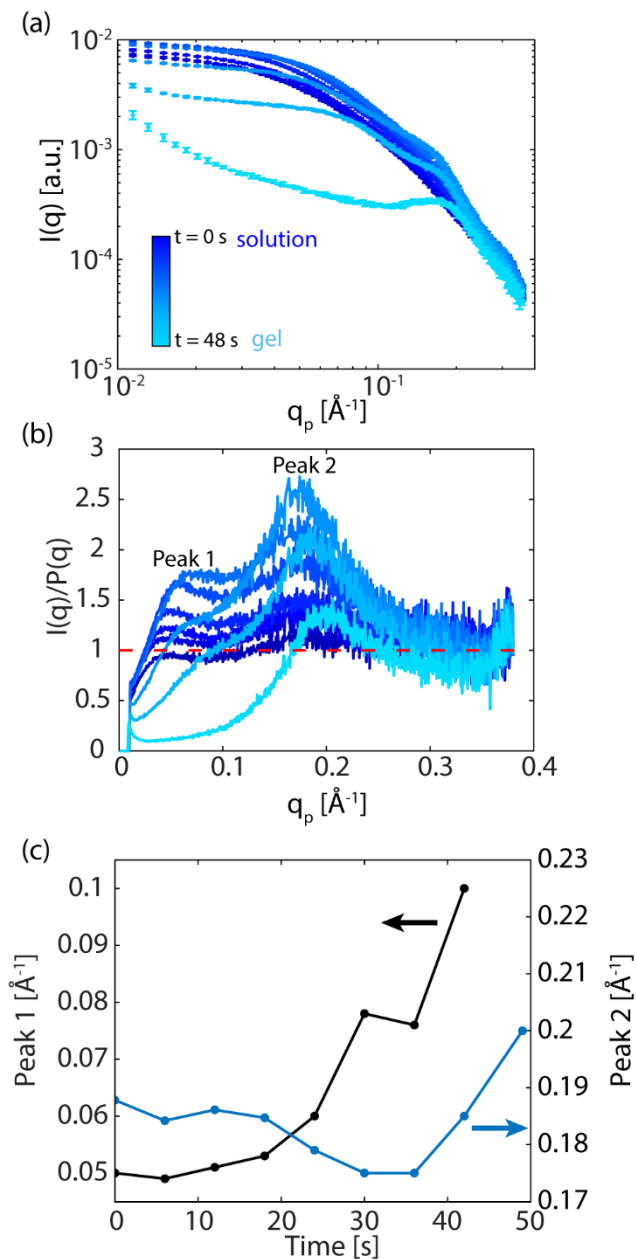

Figure 2. (a) Horizontal GISAXS linecuts showing evolution of morphology from solution to film (b) Structure factor derived from dividing intensity by core-shell cylinder form factor (c) Peak positions from (b) evolving with time.

To extract an approximate structure factor, each linecut (shown in Figure 2a) is divided by the core-shell cylinder form factor, with a length of 40nm (from previous dilute-solution studies),[23] and the cross-sectional parameters obtained from fitting the high-q region. While the aggregate length may change from dilute solution to film, the form factor in the q-region of interest is insensitive to this parameter (Figure S3). Because of this insensitivity, changes in the form factor length will not change the approximate structure factor in this q-region and for this reason we leave it constant. Two peaks are present in the structure factor (Figure 2b), and their positions vary with time (Figure 2c). As the solvent evaporates and the primary rod-like particles aggregate further, Peak 1's position monotonically increases with time, eventually collapsing as the solution transitions into a gel. This corresponds to a decrease in correlation length, i.e., d-spacing, from $d_1 \approx 12$ nm to 6 nm in less than 50 seconds. Peak 2 shows non-monotonic behavior, first moving to lower q as the solution concentrates, before quickly advancing to higher q as the solution transitions to a gel. At 48 seconds, the film is now completely in the gel state and the second peak in the solution structure factor has become the "*ionomer peak*," which is related to the hydrophilic domain spacing in the film, $d_2 \approx 3$ nm, and observed in previous GISAXS studies of spin-cast PFSA thin films.[27-28]. The evolution of the second structure factor peak into the ionomer peak highlights that the film morphology is set and mediated by interactions in ionomer solution, and by controlling these interactions one may be able to tune the final film morphology. As an example, it has been demonstrated that solvent composition affects the measured pH of PFSA dispersions, indicating differences in acid dissociation and ionomer aggregation.[24] It is expected that both the differences in solution interactions, as well as the mixed-solvent volatility, will impact the specific morphology and rate of the drying process. Subsequently, the film morphology continues to evolve slowly over the course of the next 600

6

seconds. In the film phase, the ionomer peak is fit to the Tuebner-Strey model for bi-continuous media (see SI for description),[25, 26] and the extracted parameters $(\xi, \langle \eta^2 \rangle, \kappa)$ are plotted as a function of time in Figure 3 for both through-plane (thickness direction) and in-plane (parallel to the substrate) directions.
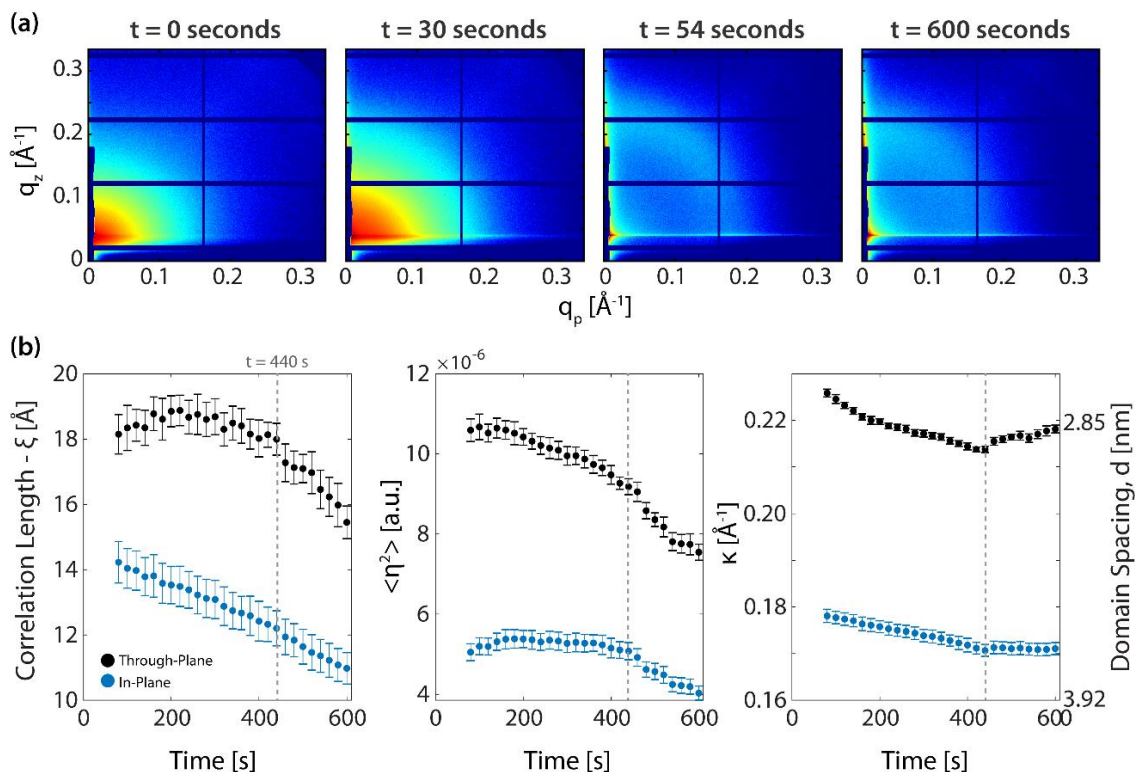

Figure 3. (a) 2D GISAXS images at selected time points (b) extracted parameters plotted as a function of time from fitting the Tuebner-Strey model to parallel and perpendicular line cuts.

In this model, ξ is the correlation length of ionomer domains and analogous to a full-width half max (FWHM) of the ionomer peak. $\langle \eta^2 \rangle$ is proportional to the scattering length contrast between phases, and κ is inversely proportional to the hydrophilic-domain spacing. Through the first 400 seconds, κ steadily decreases, corresponding to an increase domain spacing. Typically, a decrease in κ is observed as these materials hydrate with water,

corresponding to nano-swelling of hydrophilic domains.[1] Since this is occurring as solvent continues to evaporate and the film dries, it suggests that the hydrophilic domains are coalescing into fewer domains that are spaced further apart. After ~440 seconds, κ begins to increase through-plane while leveling off in-plane as the hydrophilic domains stop coalescing and the film shows usual dehydrating behavior. After this transition point, $\langle \eta^2 \rangle$ and ξ both decrease more rapidly through-plane as the contrast between hydrophilic and hydrophobic domains decreases with reduced hydration. The in-plane transition does not show such a clear change in-plane, and this may be due to the evaporative flux occurring through-plane. As such, there is less of a driving force for morphological rearrangement in the plane of the film. While domain coalescence is complete at 440 seconds, mesoscale connectivity of the hydrophilic domain-network within the film may continue to evolve through dynamic fluctuations in a chemically heterogeneous, non-equilibrium structure. Notably, the film exhibits structural anisotropy immediately upon forming a gel or film, and that anisotropy is present throughout the morphological development.

An identical sample was cast in the GIWAXS configuration to probe smaller lengthscales, particularly crystalline features (Figure 4a). PFSAs have a PTFE backbone, and crystallize into the same structure as PTFE, but with a much lower degree of crystallinity due to side-chains interrupting the hexagonal packing of backbone chains. In the dispersion state, there is initially no crystallinity. Instead, there is a peak at 0.9 Å^{-1} (d ≈ 7Å) which is part of the core-shell cylinder form factor, and a solvent correlation peak at 1.5 Å^{-1}(d ≈ 4Å). Between t = 40–60 seconds, these peaks collapse, and a convoluted amorphous and crystalline peak appears at 1.2 Å^{-1}. This crystalline peak is from the <100> lattice plane and is commonly observed in PFSAs.[1] Thus, the onset of crystallization is concurrent with the solution-to-gel transition observed in

GISAXS. The parameters extracted from the deconvoluted crystalline peak are plotted as a function of time after the first 60 seconds in Figure 4b-c. Immediately upon film formation, there is an observable orientation in the crystallites. Peak intensity is higher through-plane than in-plane, and the full-width half-max (FWHM) exhibits the opposite trend, indicating a preferential alignment of crystallites through-plane. This alignment continues to increase over time; the through-plane intensity increases, while the in-plane intensity remains constant. FWHM decreases marginally for both orientations as a function of time, indicating a slow growth in film crystallite size, a_c (which is inversely proportional to the FWHM through the relation, $a_c \propto 2\pi/\text{FWHM}$). The amorphous peak intensity decreases slightly for both orientations, again indicating marginal crystallization with time. Unlike ionomer domain coalescence, marginal crystallization appears to continue at ambient conditions very slowly, affecting the network connectivity of hydrophilic domains surrounded by the crystallites at longer lengthscales.
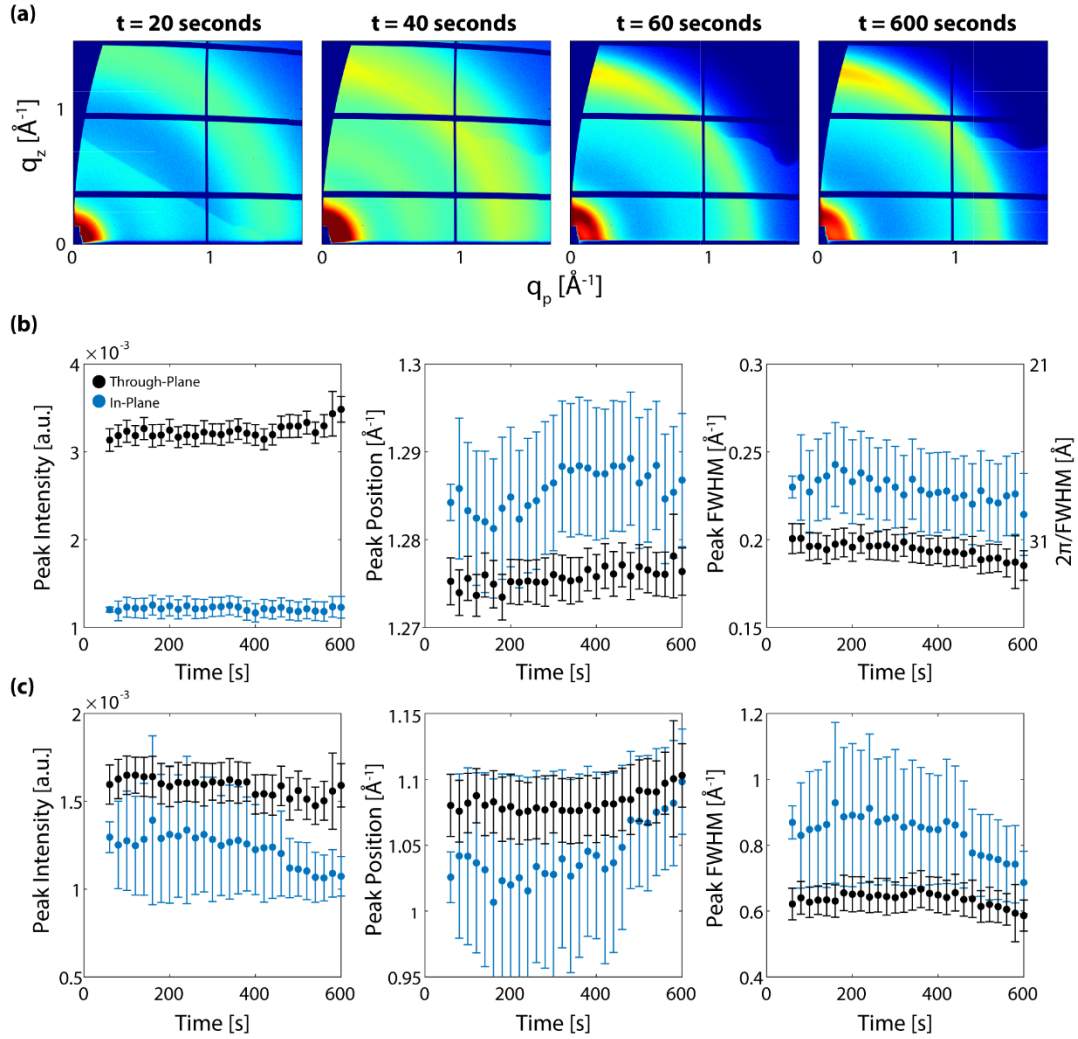
Figure 4. (a) 2D GIWAXS images at selected times, extracted (b) crystalline and (c) amorphous parameters as a function of time. A double-Gaussian was used to fit and deconvolute amorphous and crystalline peaks.

With the two experiments probing multiple lengthscales of ionomer film formation, a picture of the overall morphology emerges (Figure 5). The film formation of PFSA ionomer cast via slot-die printing proceeds through four stages: I. *Solution phase*, II. *Sol-Gel transition*, III. *Gel phase*, IV. *Film drying*. In Stage-I as the film is initially cast, solvent evaporates, concentrating the solution and inducing further primary particle aggregation. No backbone crystallinity is observed in this first stage. Then, the solution concentrates to a point where ionomer aggregates

percolate into a gel-like phase and the structure factor peaks begin to collapse into the ionomer peak (Stage-II). In this stage (II), GIWAXS data shows the onset of crystallization and the convoluted amorphous/crystalline peak from the ionomer backbone is present in the GIWAXS patterns. The majority of crystallization is completed in Stage-II, although the crystallites continue to ripen marginally through stages III-IV. In Stage-III, the ionomer domains coalesce, forming fewer domains that are spaced further apart. Thus, the decrease in κ, which proceeds steadily until Stage-IV, where the film exhibits drying behavior as the hydrophilic domains shrink and move closer together. While domain coalescence is complete at the end of Stage-III, crystallites continue to develop through Stage-IV and beyond the timescale of the experiment, impacting overall crystallinity and perhaps network connectivity.

Throughout the film formation process, there is an anisotropy in both the ionomer and crystalline peaks, highlighting the impact of confinement on the system. Crystallites are preferentially aligned through-plane and the ionomer domains are spaced closer through-plane, which has implications for water and ion transport and subsequently catalyst layer performance. While preferential orientation of domains has been reported in spin-cast thin-films,[2, 27-31] this study reveals that the origin of such structural anisotropy is rooted in the film formation, during which crystallites and nano-domains orient with the substrate. Likely, this is due to the stiff rod-like aggregates aligning parallel to both interfaces as the solution evaporates and transitions into a thin film. The preferential interaction of ionomer moieties with the substrate interface through the ionic groups facilitate this alignment of the backbone chains constituting the polymer aggregates.[32] Prior work has demonstrated anisotropic transport and proton conductivity in ionomer thin-films,[33-35] accompanied by higher stiffness,[6] which is attributed to preferential alignment of domains within the film.[28, 30-34, 36] Controlling this alignment and ultimately the

phase-separated morphology is important for improving catalyst-layer performance, and how to
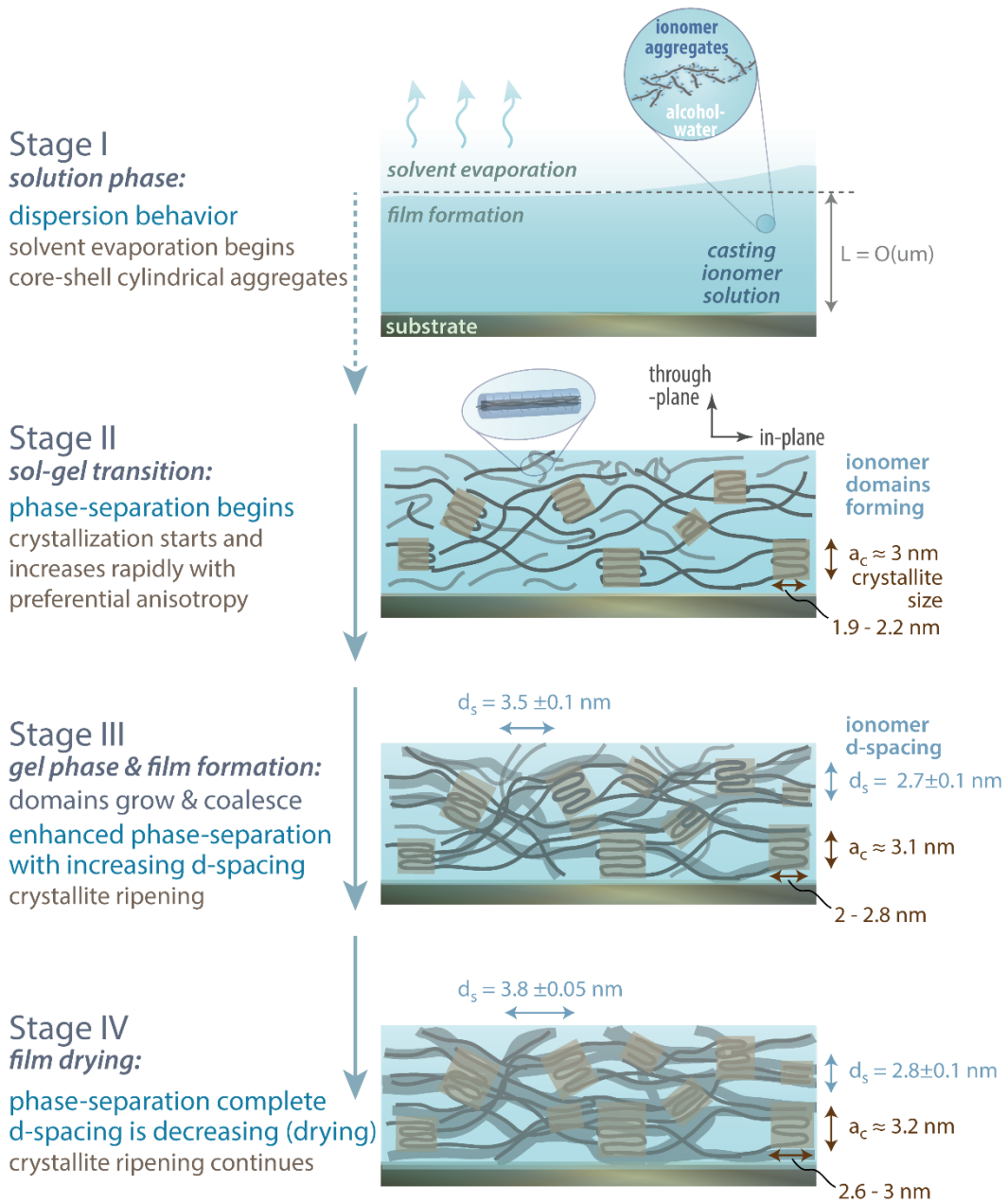
achieve tunability is an open question.

Figure 5. Illustration of the evolution of morphological features during formation of a PFSA thin-film from a dispersion based on the time-resolved GI(SAXS-WAXS) data.

Findings herein illustrate the key role of film formation during casting in setting a morphology, which indicates tuning of ionomer-solvent interactions, processing via casting method, and temperature control as possible routes to control film functionality.

The fact that hydrophobic semi-crystalline domains and polar domains evolve at different timescales during film formation underscores the key role of ionomer's chemically dissimilar phases and their preferential interactions with the solvents (*e.g.,* alcohol vs. water) in morphology. To demonstrate this further, we cast Nafion films from different solvent ratios of water to n-propanol (nPA) at the same weight percent and have plotted horizontal GISAXS linecuts with time (Figure 6). Across the three solvent ratios, all show markedly different transitions from solution to film and reach their gel point at different times. This gelation time scales with increasing water content in the solution; less volatile mixtures have a lower evaporative driving force. In addition, the structure factor peaks across the samples all differ due to local solvent environment around the ionic group. These differences subsequently lead to varying interaction strengths and degrees of aggregate ordering. While the impact of these structural changes on properties warrant further investigation, the solvent type and composition appears to have a significant impact on the evolution of morphology from solution to film.
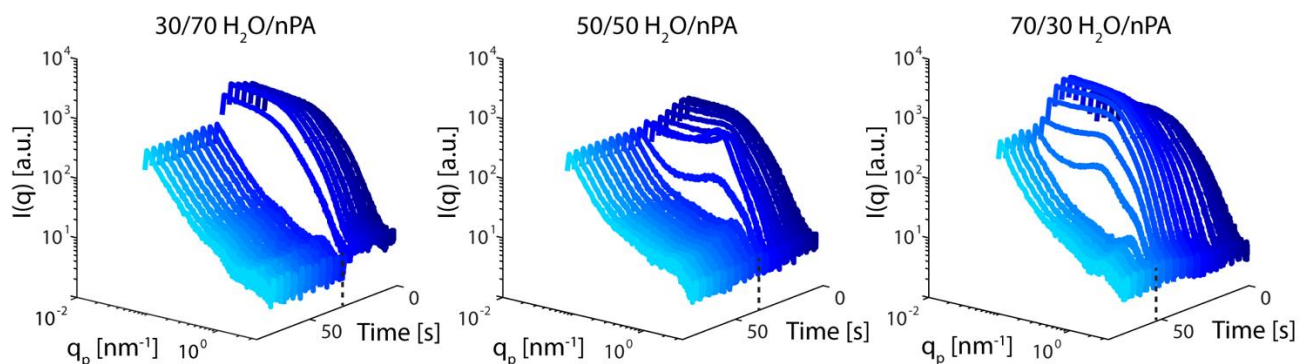
Figure 6- in-situ GISAXS casting of different solvent ratios, demonstrating the effect of solvent composition on non-equilibrium morphology evolution. Dashed lines in each plot denote the time at which the film transitions from solution to gel

To conclude, the continued ripening of crystallites beyond the timescale of the initial experiment, along with their preferential orientation, brings up the questions of film aging and long-term relaxation, and how they impact film behavior and functionality. Demonstration of this powerful technique for ionomer film formation serves as a baseline for subsequent studies to explore roles of materials and processing parameters in understanding and manipulating structure-functionality of ion-exchange thin-films for various technologies, including the electrodes of energy conversion devices.

Experimental Section

Ionomer solutions. Nafion®-ionomer dispersion (5-wt% solids of 1100 g polymer $(molSO_3^-)^{-1}$ in alcohol-water mixture) were obtained from Sigma Aldrich. (St. Louis, MO) and used as purchased. For the solvent ratio dispersions, Nafion D2021 (20-wt% solids of 1100 g polymer $(molSO_3^-)^{-1}$ in alcohol-water mixture) was diluted in varying water/nPA ratios to 4-wt% solids. Nafion D2021 was purchased from Ion-Power Inc. (New Castle, DE).

Thin-film Casting. PFSA thin-films were cast in-situ using a custom-built mini slot-die printer.[13] After priming the line with solution, the films were cast from the slot-die head onto a silicon wafer

with a head-substrate gap height of 50 um and an injection rate of 5 uL/s. The print head was stationary while the substrate was translated underneath at a rate of 5 mm/s.

Grazing-incidence X-ray Scattering (GISAXS/GIWAXS). GISAXS/GIWAXS measurements were performed at beamline 7.3.3 of the ALS at LBNL.[37] The X-ray energy was 10 keV (λ=1.24 A^{-1}) with a monochromator energy resolution E/dE of 100, and the patterns were acquired with a Dectris Pilatus 1M or 2M CCD area detector (172 μm x 172 μm pixel size). GISAXS images were collected at grazing incidence angles (α_i) of 0.18° with 2 sec exposure. GIWAXS images were collected under He at $\alpha_i = 0.16°$ with a 3 second exposure time and corrected to account for the missing wedge of the Ewald sphere. Through-plane intensity vs. scattering wave vector I(q) profiles were obtained from 1° sector cuts and in-plane I(q) profiles were obtained using horizontal line-cuts ($\Delta q = 0.278 \, nm^{-1}$). The core-shell cylinder form factor was fit in the SANS Toolbox within Igor Pro[38] and the Tuebner-Strey and double Gaussian models were fit using scripts written in Matlab. Error bars on the extracted parameters represent a 95% confidence interval. Exposure times and total dose were selected to mitigate x-ray induced damage to the sample. Included in the supplementary information is a more detailed discussion on Distorted Wave Born Approximation effects, fitting, and the models used in this work.

Supporting Information:

Associated Content: Full experimental methods and detailed discussion of the modeling of scattering data.

References

1.   Kusoglu, A.; Weber, A. Z. New Insights into Perfluorinated Sulfonic-Acid Ionomers. *Chemical Reviews* **2017,** 117 (3), 987-1104.
2.   Kusoglu, A., Ionomer Thin Films in PEM Fuel Cells. In *Encyclopedia of Sustainability Science and Technology*, Meyers, R. A., Ed. Springer New York: New York, NY, 2018; pp 1-23.
3.   Holdcroft, S. Fuel Cell Catalyst Layers: A Polymer Science Perspective. *Chemistry of Materials* **2014,** 26 (1), 381-393.
4.   Hatzell, K. B.; Dixit, M. B.; Berlinger, S. A.; Weber, A. Z. Understanding inks for porous-electrode formation. *Journal of Materials Chemistry A* **2017,** 5 (39), 20527-20533.
5.   Karan, K. PEFC catalyst layer: Recent advances in materials, microstructural characterization, and modeling. *Current Opinion in Electrochemistry* **2017,** 5 (1), 27-35.
6.   Page, K. A.; Kusoglu, A.; Stafford, C. M.; Kim, S.; Kline, R. J.; Weber, A. Z. Confinement-driven increase in ionomer thin-film modulus. *Nano letters* **2014,** 14 (5), 2299-304.

7.   Welch, C.; Labouriau, A.; Hjelm, R.; Orler, B.; Johnston, C.; Kim, Y. S. Nafion in Dilute Solvent Systems: Dispersion or Solution? *ACS Macro Lett* **2012,** 1 (12), 1403-1407.

8.   Shibayama, M.; Matsunaga, T.; Kusano, T.; Amemiya, K.; Kobayashi, N.; Yoshida, T. SANS Studies on Catalyst Ink of Fuel Cell. *J Appl Polym Sci* **2014,** 131 (3), 39842.

9.   Yamaguchi, M.; Matsunaga, T.; Amemiya, K.; Ohira, A.; Hasegawa, N.; Shinohara, K.; Ando, M.; Yoshida, T. Dispersion of Rod-like Particles of Nafion in Salt-Free Water/1-Propanol and Water/Ethanol Solutions. *J Phys Chem B* **2014,** 118 (51), 14922-8.

10.   Kim, Y. S.; Welch, C. F.; Hjelm, R. P.; Mack, N. H.; Labouriau, A.; Orler, E. B. Origin of Toughness in Dispersion-Cast Nafion Membranes. *Macromolecules* **2015,** 48 (7), 2161-2172.

11.   Konosu, Y.; Masunaga, H.; Hikima, T.; Tokita, M.; Matsumoto, H.; Sasabe, T.; Yoshida, T.; Shinohara, K.; Hirai, S. Time-Resolved Nanostructural Analysis of Thin-Film Formation Process from Nafion Solution by Synchrotron X-Ray Scattering. *ECS Transactions* **2016,** 75 (14), 637-642.

12.   Konosu, Y.; Koga, M.; Matsumoto, H.; Tokita, M.; Masunaga, H.; Hikima, T.; Sugimori, H.; Yoshida, T.; Shinohara, K.; Hirai, S. Time-Resolved Nanostructural Analysis of Catalyst Layer Formation Process by Synchrotron X-ray Scattering. *ECS Transactions* **2017,** 80 (8), 269-273.

13.   Liu, F.; Ferdous, S.; Schaible, E.; Hexemer, A.; Church, M.; Ding, X.; Wang, C.; Russell, T. P. Fast Printing and In Situ Morphology Observation of Organic Photovoltaics Using Slot-Die Coating. *Advanced Materials* **2015,** 27 (5), 886-891.

14.   Pröller, S.; Liu, F.; Zhu, C.; Wang, C.; Russell, T. P.; Hexemer, A.; Müller-Buschbaum, P.; Herzig, E. M. Following the Morphology Formation In Situ in Printed Active Layers for Organic Solar Cells. *Advanced Energy Materials* **2016,** 6 (1), 1501580.

15.   M., P. C.; Feng, L.; P., R. T.; Alexander, H.; Cheng, W.; Peter, M. B. The Crystallization of PEDOT:PSS Polymeric Electrodes Probed In Situ during Printing. *Advanced Materials* **2015,** 27 (22), 3391-3397.

16.   Manley, E. F.; Strzalka, J.; Fauvell, T. J.; Jackson, N. E.; Leonardi, M. J.; Eastham, N. D.; Marks, T. J.; Chen, L. X. In Situ GIWAXS Analysis of Solvent and Additive Effects on PTB7 Thin Film Microstructure Evolution during Spin Coating. *Adv Mater* **2017,** 29 (43), 1703933.

17.   Chou, K. W.; Yan, B.; Li, R.; Li, E. Q.; Zhao, K.; Anjum, D. H.; Alvarez, S.; Gassaway, R.; Biocca, A.; Thoroddsen, S. T.; Hexemer, A.; Amassian, A. Spin-Cast Bulk Heterojunction Solar Cells: A Dynamical Investigation. *Advanced Materials* **2013,** 25 (13), 1923-1929.

18.   Al-Hussein, M.; Herzig, E. M.; Schindler, M.; Löhrer, F.; Palumbiny, C. M.; Wang, W.; Roth, S. V.; Müller-Buschbaum, P. Comparative study of the nanomorphology of spray and spin coated PTB7 polymer: Fullerene films. *Polymer Engineering & Science* **2016,** 56 (8), 889-894.

19.   Liu, F.; Gu, Y.; Jung, J. W.; Jo, W. H.; Russell, T. P. On the morphology of polymer-based photovoltaics. *J Polym Sci Pol Phys* **2012,** 50 (15), 1018-1044.

20.   Gebel, G.; Loppinet, B. Colloidal structure of ionomer solutions in polar solvents. *J Mol Struct* **1996,** 383 (1-3), 43-49.

21.   Rubatat, L.; Gebel, G.; Diat, O. Fibrillar Structure of Nafion: Matching Fourier and Real Space Studies of Corresponding Films and Solutions. *Macromolecules* **2004,** 37 (20), 7772-7783.

22.   Gebel, G. Structural evolution of water swollen perfluorosulfonated ionomers from dry membrane to solution. *Polymer* **2000,** 41 (15), 5829-5838.

23.   Loppinet, B.; Gebel, G.; Williams, C. E. Small-Angle Scattering Study of Perfluorosulfonated Ionomer Solutions. *The Journal of Physical Chemistry B* **1997,** 101 (10), 1884-1892.

24. Berlinger, S. A.; McCloskey, B. D.; Weber, A. Z. Inherent Acidity of Perfluorosulfonic Acid Ionomer Dispersions and Implications for Ink Aggregation. *The Journal of Physical Chemistry B* **2018,** 122 (31), 7790-7796.

25. Teubner, M.; Strey, R. Origin of the Scattering Peak in Microemulsions. *J Chem Phys* **1987,** 87 (5), 3195-3200.

26. Chen, S. H.; Chang, S. L.; Strey, R. In *On the interpretation of scattering peaks from bicontinuous microemulsions*, Darmstadt, 1990; Steinkopff: Darmstadt, 1990; pp 30-35.

27. DeCaluwe, S. C.; Kienzle, P. A.; Bhargava, P.; Baker, A. M.; Dura, J. A. Phase segregation of sulfonate groups in Nafion interface lamellae, quantified via neutron reflectometry fitting techniques for multi-layered structures. *Soft Matter* **2014,** 10 (31), 5763-76.

28. Dura, J. A.; Murthi, V. S.; Hartman, M.; Satija, S. K.; Majkrzak, C. F. Multilamellar Interface Structures in Nafion. *Macromolecules* **2009,** 42 (13), 4769-4774.

29. Modestino, M. A.; Kusoglu, A.; Hexemer, A.; Weber, A. Z.; Segalman, R. A. Controlling Nafion Structure and Properties via Wetting Interactions. *Macromolecules* **2012,** 45 (11), 4681-4688.

30. Kusoglu, A.; Kushner, D.; Paul, D. K.; Karan, K.; Hickner, M. A.; Weber, A. Z. Impact of Substrate and Processing on Confinement of Nafion Thin Films. *Adv Funct Mater* **2014,** 24 (30), 4763-4774.

31. Kusoglu, A.; Dursch, T. J.; Weber, A. Z. Nanostructure/Swelling Relationships of Bulk and Thin-Film PFSA Ionomers. *Adv Funct Mater* **2016,** 26 (27), 4961-4975.

32. Kushner, D. I.; Kusoglu, A.; Podraza, N. J.; Hickner, M. A. Substrate-Dependent Molecular and Nanostructural Orientation of Nafion Thin Films. *Adv Funct Mater* **2019,** 0 (0), 1902699.

33. Nagao, Y. Proton-Conductivity Enhancement in Polymer Thin Films. *Langmuir* **2017,** 33 (44), 12547-12558.

34. Dishari, S. K.; Hickner, M. A. Confinement and Proton Transfer in NAFION Thin Films. *Macromolecules* **2013,** 46 (2), 413-421.

35. Ogata, Y.; Abe, T.; Yonemori, S.; Yamada, N. L.; Kawaguchi, D.; Tanaka, K. Impact of the Solid Interface on Proton Conductivity in Nafion Thin Films. *Langmuir* **2018,** 34 (50), 15483-15489.

36. Tesfaye, M.; Kushner, D. I.; Kusoglu, A. Interplay between Swelling Kinetics and Nanostructure in Perfluorosulfonic Acid Thin-Films: Role of Hygrothermal Aging. *ACS Applied Polymer Materials* **2019,** 1 (4), 631-635.

37. Hexemer, A.; Bras, W.; Glossinger, J.; Schaible, E.; Gann, E.; Kirian, R.; MacDowell, A.; Church, M.; Rude, B.; Padmore, H. A SAXS/WAXS/GISAXS Beamline with Multilayer Monochromator. *Journal of Physics: Conference Series* **2010,** 247, 012007.

38. Kline, S. Reduction and analysis of SANS and USANS data using IGOR Pro. *Journal of Applied Crystallography* **2006,** 39 (6), 895-900.

For Table of Contents Only